International Journal of Pharmaceutics: X 2 (2020) 100049

Contents lists available at ScienceDirect

International Journal of Pharmaceutics: X

journal homepage: www.journals.elsevier.com/international-journal-of-pharmaceutics-x

Polymeric micelles loaded with carfilzomib increase tolerability in a humanized bone marrow-like scaffold mouse model

Aida Varela-Moreira[a,b], Demian van Straten[a], Heleen F. van Leur[b], Ruud W.J. Ruiter[c], Anil K. Deshantri[a,d], Wim E. Hennink[b], Marcel H.A.M. Fens[b], Richard W.J. Groen[c], Raymond M. Schiffelers[a,b,*]

[a] Laboratory of Clinical Chemistry and Hematology (LKCH), University Medical Center Utrecht, Heidelberglaan 100, 3584, CX, Utrecht, the Netherlands
[b] Department of Pharmaceutics, Utrecht Institute for Pharmaceutical Sciences (UIPS), Faculty of Science, Utrecht University, Universiteitsweg 99, 3584, CG, Utrecht, the Netherlands
[c] Department of Hematology, Amsterdam UMC, VU University Medical Center, Cancer Center Amsterdam, De Boelelaan 1118, 1182, DB, Amsterdam, the Netherlands
[d] Biological Research Pharmacology Department, Sun Pharma Advanced Research Company Ltd., Vadodara, India

ARTICLE INFO

Keywords:
Polymeric micelles
Carfilzomib
Drug delivery
Proteasome inhibitor
Multiple Myeloma
Bone Marrow Microenvironment

ABSTRACT

Carfilzomib-loaded polymeric micelles (CFZ-PM) based on poly(ethylene glycol)-b-poly(N-2-benzoyloxypropyl methacrylamide) (mPEG-b-p(HPMA-Bz)) were prepared with the aim to improve the maximum tolerated dose of carfilzomib in a "humanized" bone marrow-like scaffold model. For this, CFZ-PM were prepared and characterized for their size, carfilzomib loading and cytotoxicity towards multiple myeloma cells. Further, circulation and tumor & tissue distribution of fluorescently labeled micelles were determined. Tolerability of CFZ-PM *versus* the clinical approved formulation – Kyprolis® – was assessed. CFZ-PM presented small diameter below 55 nm and low PDI < 0.1. Cy7-labeled micelles circulated for extended periods of time with over 80% of injected dose in circulation at 24 h after intravenous injection and 1.3% of the injected dose of Cy7-labeled micelles accumulated in myeloma tumor-bearing scaffolds. Importantly, CFZ-PM were well tolerated whereas Kyprolis® showed adverse effects. Kyprolis® dosed at the maximum tolerated dose, as well as CFZ-PM, did not show therapeutic benefit, while multiple myeloma cells showed sensitivity *in vitro*, underlining the importance of the bone marrow crosstalk in testing novel formulations. Overall, this work indicates that PM are potential drug carriers of carfilzomib.

1. Introduction

Multiple Myeloma (MM) is one of the most common types of cancer, accounting for 1% of all cancers and 13% of blood cancers (Palumbo and Anderson, 2011). The median age at diagnosis is 70 years. MM is a hematologic cancer resulting from a clonal expansion of plasma cells in the bone marrow (BM) (Roodman, 2009) and clinically characterized by the following symptoms: high Calcium levels, Renal damage, Anemia and Bone lesions – collectively known as the CRAB features.

Conventional treatments include combination of melphalan and prednisone or high dose chemotherapy combined with stem cell transplantation (Azaïs et al., 2010). Although MM remains an incurable disease, progress has been made with the introduction of novel therapeutic agents that improve the median recurrence free survival. New targeted treatments such as immunomodulatory agents (*e.g.* thalidomide, lenalidomide and pomalidomide) and proteasome inhibitors (*e.g.* bortezomib, carfilzomib and ixazomib) (Gandolfi et al., 2017; Okazuka and Ishida, 2018) given in combination with classical chemotherapeutics such as melphalan and cyclophosphamide have further increased the survival rate and in general improve patients' quality of life [3,6]. Particularly proteasome inhibitors have shown an added advantage. This class of agents play a role in the disruption of the ubiquitin proteasome pathway thereby causing accumulation of damaged/misfolded proteins, pro-apoptotic proteins, cyclins and inhibition of NF-kB signaling among others (Okazuka and Ishida, 2018). This leads to a cell cycle arrest and eventually apoptosis. Interestingly, malignant cells were shown to be more sensitive to proteasome inhibitors than healthy cells which make them a valuable therapeutic option (Adams, 2004).

Carfilzomib (structure shown in Fig. 1 A), a second generation

* Corresponding author at: Laboratory of Clinical Chemistry and Hematology (LKCH), Room G 03.647, University Medical Center Utrecht, Heidelberglaan 100, 3584 CX, PO Box 85500, 3508 GA Utrecht, the Netherlands.
E-mail address: r.schiffelers@umcutrecht.nl (R.M. Schiffelers).

https://doi.org/10.1016/j.ijpx.2020.100049
Received 5 February 2020; Received in revised form 6 May 2020; Accepted 8 May 2020
Available online 16 May 2020

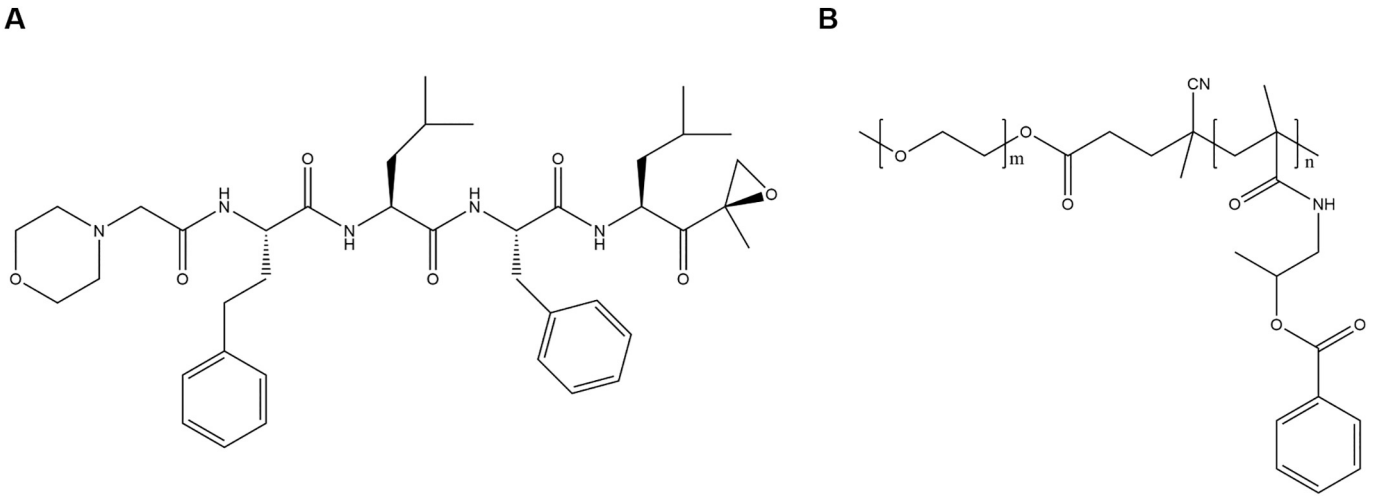

Fig. 1. Chemical structure of (A) carfilzomib and (B) mPEG-b-p(HPMA-Bz) copolymer (Total Mn = 22 kDa, mPEG of 5 kDa) prepared with HPMA-Bz as monomer and mPEG2-ABCPA as initiator.

proteasome inhibitor, is a tetrapeptide bearing an epoxyketone that covalently and irreversibly binds to the beta- 5 subunit of the proteasome (Andreu-Vieyra and Berenson, 2014). Clinical studies showed that relapsed or refractory patients, including those that failed to respond to the CFZ-analogue bortezomib, would still benefit from treatment with CFZ (Kumar et al., 2012; Papadopoulos et al., 2015). However, the administration of proteasome inhibitors is associated with several limitations as the poor water solubility (FDA, 2012), fast clearance (Wang et al., 2013a, 2013b) and adverse effects (Harvey, 2014). Due to its limited solubility in aqueous solutions (FDA, 2012), CFZ depends on a vehicle to solubilize and enable systemic administration. In 2012, a formulation of CFZ (Kyprolis®) was approved by the FDA for the treatment of relapsed or refractory MM patients as single agent (Herndon et al., 2013). Kyprolis® consists of CFZ complexed in sulfobutylether beta-cyclodextrin (Captisol®) to allow systemic administration (2% in weight CFZ). However, Kyprolis® has a poor pharmacokinetic profile with a half-life of 30 min after intravenous (i.v.) injection, and is also rapidly metabolized mainly *via* extrahepatic peptidase cleavage and inactivated by epoxide hydrolysis (Yang et al., 2011; Papadopoulos et al., 2013; Papadopoulos et al., 2015). As a result, high dosing and multiple administration are needed to achieve therapeutic benefits.

These issues highlight the need of developing delivery systems for proteasome inhibitors to expedite their use in a clinical setting. Several recent studies report the development of delivery systems for proteasome inhibitors that increase their therapeutic value (Park et al., 2017; Gu et al., 2018). We have previously identified π-π stacked polymeric micelles based on poly(ethylene glycol)-b-poly(N-2-benzoyloxypropyl methacrylamide) (mPEG-b-p(HPMA-Bz) (structure shown in Fig. 1B) that allow long-circulation of paclitaxel and showed tumor regression in two solid tumor models (Shi et al., 2015). This micellar system has also shown therapeutic advantages over liposomes and lipoprotein-based nanoparticles in a mouse model of atherosclerosis, leading to a decrease of macrophage burden within atherosclerotic plaques (Alaarg et al., 2017). Similar to paclitaxel, CFZ contains aromatic moieties and we therefore hypothesized that CFZ can be efficiently accommodated and retained in π-π stacked polymeric micelles.

Importantly, a suitable MM model is needed to evaluate the therapeutic potential of CFZ-loaded micelles (CFZ-PM). In MM, the BM microenvironment is of utmost importance for the support and maintenance of myeloma cells (Manier et al., 2012). Malignant plasma cells interact with cellular and non-cellular components of the BM microenvironment, which leads to the release of soluble factors that in turn result in survival and/or proliferation of these cells. Taking this into account, the development of suitable mouse models that review the alliance of tumor cells and supporting/surrounding cells for drug testing is key.

Here, we used a "humanized" BM-like scaffold (huBMsc) model, an advanced mouse model of MM dependent on tissue-engineering of bone on ceramic material in immunodeficient RAG2$^{-/-}\gamma c^{-/-}$ mice (Prins et al., 2009; Groen et al., 2012). In short, calcium phosphate scaffolds are seeded with human mesenchymal stem cells (hMSCs), which after *in vitro* osteogenic differentiation and subcutaneous implantation develop into a BM-like environment that is well vascularized and has shown to support MM outgrowth. This human-mouse hybrid animal model has shown to closely resemble the actual disease and accurately predict individual patient response in a personalized medicine set-up (Groen et al., 2012). In the present work, we investigated loading and retention of carfilzomib in π-π stacked polymeric micelles and compared it to the clinical approved formulation - Kyprolis®. Subsequently, circulation time and tissue disposition profile of labeled polymeric micelles was assessed. Finally, the therapeutic potential and tolerability of CFZ-PM were evaluated.

2. Materials and methods

2.1. Preparation and characterization of carfilzomib-loaded polymeric micelles

CFZ-PM were prepared by nanoprecipitation. In brief, mPEG-b-p (HPMA-Bz) copolymer (total M_n of 22 kDa, mPEG of 5 kDa) prepared with HPMA-Bz as monomer and $mPEG_2$-ABCPA as initiator (Bagheri et al., 2018) and carfilzomib (LC laboratories; Woburn, USA) were dissolved in THF (Biosolve BV, Valkenswaard, the Netherlands). Briefly, 30 mg of copolymer and 1 mg of carfilzomib were dissolved in 1 mL of THF and subsequently added dropwise to 1 mL of water while stirring. The sample was placed in the fume hood overnight to allow organic solvent evaporation. After 16 h, the volume of the micellar dispersion was adjusted to 1 mL with a concentrated solution of HEPES Buffered Saline (HBS), 200 mM HEPES, 1500 mM NaCl, pH 7.4, in order to obtain a micellar dispersion with a final concentration of 20 mM HEPES, 150 mM NaCl, pH 7.4. Subsequently, the micelles were filtered through a 0.45 μm pore size filter (Phenomenex Inc., USA) to remove non-entrapped/precipitated drug. Cy7-labeled micelles (Cy7-PM) were prepared as described above by blending Cy7-labeled mPEG-b-p (HPMA-Bz) (1.5% in weight) (Shi et al., 2015) with non-labeled mPEG-b-p(HPMA-Bz). Size of CFZ-PM was determined by Dynamic Light Scattering after 10× dilution in water at 25 °C (ZetaSizer Nano ZS 90,

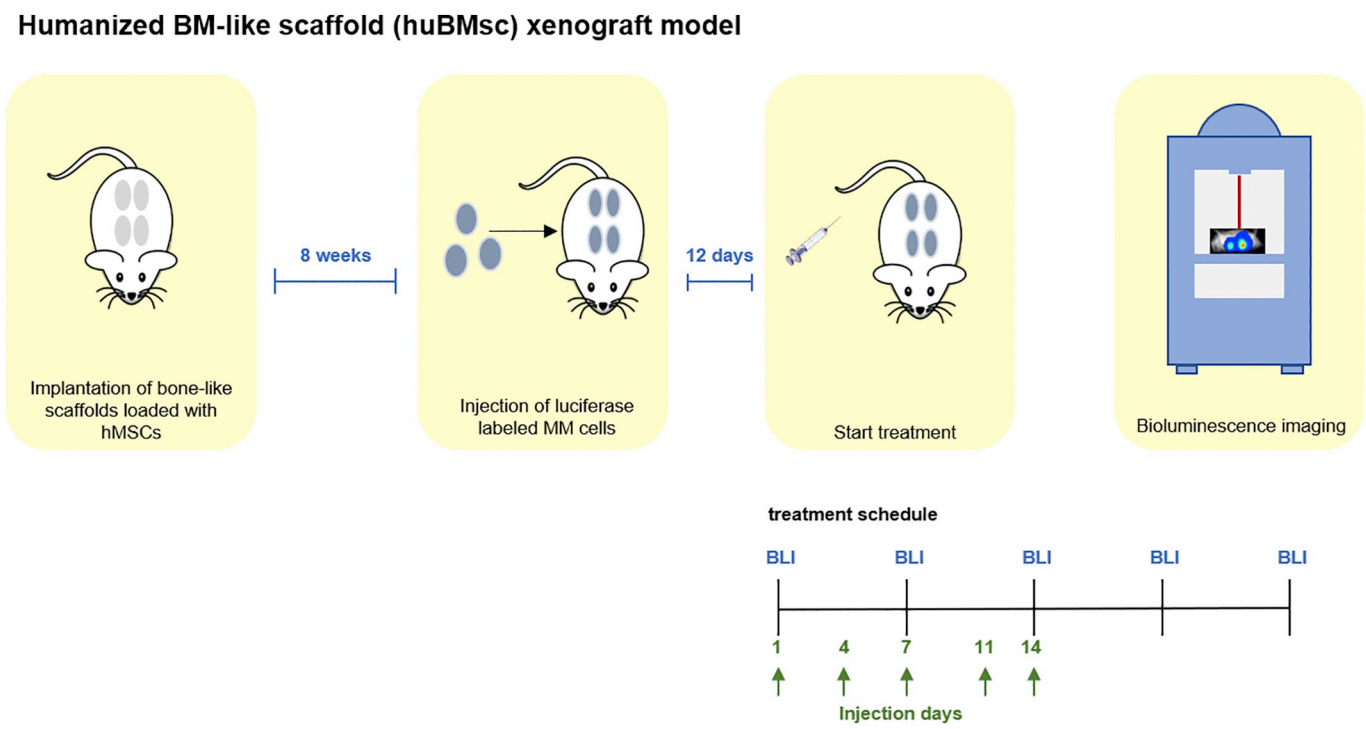

Fig. 2. Schematic representation of "humanized" BM-like scaffold (huBMsc) xenograft model and treatment schedule. Eight weeks after implantation of bone-like scaffolds (4 per mouse) seeded with hMSCs, MM.1S cells were inoculated into the scaffolds. Treatments started twelve days after MM.1S cells inoculation. Formulations were i.v. administered twice a week, with a total of five injections per mouse. Bioluminescence imaging was performed every week up to four weeks from start of the treatment.

Malvern Analytical, UK). Mean Z-averaged particle size and polydispersity index (PDI) were obtained from analysis of supplier's software. To assess CFZ content, micelles were diluted 10× in acetonitrile and briefly vortexed. CFZ content was determined by ultra-high-performance liquid chromatography (UPLC) using a Waters ACQUITY system (Waters Associates Inc., Milford, MA, USA) equipped with a C18 column (ACQUITY UPLC BEHC18 1.7 µm, 2.1 × 50 mm). In brief, a gradient was run starting with 35% of eluent B and 65% of eluent A and increasing to 70% B and 30% A in 3 min. This fraction was kept until 4.7 min. Then, the volume fraction of eluent B decreased again to 35% from 4.7 to 6.2 min. Eluent A was 2 mM ammonium formate in water and eluent B acetonitrile (Sestak et al., 2016). Run time was 7 min, injection volume was of 7.5 µL and wavelength for detection was 220 nm. Flow rate was set to 0.4 mL/min and column temperature was 30 °C. CFZ calibration was done in water/acetonitrile (1:1, *v*/v) at concentrations ranging from 0.25–250 µg/mL. Chromatograms were analyzed using Empower Software.

2.2. Retention of carfilzomib in polymeric micelles

CFZ-PM samples (1 mL) were transferred inside a dialysis cassette (Float-a-Lyzer G2 100 kDa MWCO, Repligen Corporation, Boston, MA, USA). Dialysis was performed against a 30 mL solution of 2% (*v*/v) of Triton X-100 (Sigma-Aldrich Zwijndrecht, the Netherlands) in PBS at 4 or 37 °C for 24 h (Naksuriya et al., 2015). As control, release was also conducted only in PBS at 37 °C for 24 h. Dialysis samples were treated the same as the micelles, and diluted 10× with acetonitrile. Release of CFZ-PM in bovine serum albumin (Sigma-Aldrich Zwijndrecht, the Netherlands) (40 mg/mL) was conducted similarly, but with a Float-a-Lyzer of 300 kDa MWCO (Repligen Corporation, Boston, MA, USA). An excess of albumin compared to CFZ was used, at a molar ratio of 1300:1, albumin:CFZ. The collected samples were diluted 10× with acetonitrile and centrifuged at 12,000*g* for 10 min to precipitate and separate albumin from CFZ. The supernatant was collected, and water added to have a final concentration of 50% acetonitrile in the sample for injection in UPLC.

2.3. Effect of carfilzomib (free and formulations) on multiple myeloma cells viability in vitro

Cytotoxic effect of CFZ-PM, CFZ-CD and CFZ free was assessed on different MM cell lines. Luciferase transduced MM cell lines were generated as described previously (Groen et al., 2012). MM1.S, L363 and UM-9 were cultured in Greiner CELLSTAR® T75 flasks with RPMI-1640 medium supplemented with 20% fetal bovine serum (FBS) and 1% antibiotics (penicillin/streptomycin). Cells were kept in culture at 37 °C in a humidified atmosphere containing 5% CO_2. Cells were seeded in Greiner CELLSTAR® 96-well plates at a density of 6250 cells per well. On the same day, cells were incubated with solutions of increasing concentrations (0.8–20 nM) of carfilzomib in DMSO (CFZ free), in sulfobutylether β-cyclodextrin (CFZ-CD), prepared likewise Kyprolis®, or in polymeric micelles (CFZ-PM) for 48 h at 37 °C in a humidified atmosphere containing 5% CO_2. As control, empty PM prepared at polymer concentrations ranging from 1 to 100 µg/mL were also added to cells. After incubation, beetle luciferin (Promega, US) was added to each well at final concentration of 3 mM. After 10 min, luminescence was detected (SpectraMax M2e, Molecular Devices, Canada). The percentage of viable cells was calculated and compared to control (untreated) wells. All products, otherwise mentioned, were supplied by Sigma-Aldrich (Zwijndrecht, the Netherlands).

2.4. Humanized BM-like scaffold (huBMsc) xenograft model

Female RAG2$^{-/-}\gamma c^{-/-}$ mice were kept in standard housing on a 12 h light/dark cycle with free access to water and food. Human bone-like scaffolds (four per mice) of 2- to 3-mm biphasic calcium phosphate particles were prepared as previously described (Yuan et al., 2002; Prins et al., 2009). Scaffolds were implanted subcutaneously into the

back side of RAG2$^{-/-}\gamma c^{-/-}$ mice (Groen et al., 2012) and loaded with hMSCs injected directly into the bone structures (Fig. 2). After at least eight weeks of implantation, mice were intraperitoneally injected with Busilvex® (18 mg/kg) to prevent rejection of cell transplantation. Next day, scaffolds were injected with luciferase expressing MM.1S cells (1×10^6 cells/scaffold). Treatment started 12 days after tumor cells inoculation. The animal experiments were performed with permission from the local ethical committee for animal experimentation and were following the Dutch Animal Experimentation Act.

2.4.1. In vivo circulation kinetics and biodistribution of Cy7-labeled polymeric micelles

For circulation and biodistribution studies, mice were i.v. injected with 100 μL of empty Cy7-PM (30 mg/mL of mPEG-b-p(HPMA-Bz) containing 1.5 wt% of Cy7-labeled polymer) *via* the tail vein. Blood was withdrawn at 1 min, 1 and 2 h after injection, by puncture of the submandibular vein and at 4 and 24 h *via* cardiac puncture when mice were sacrificed *via* CO_2 asphyxiation. Blood collected in heparinized tubes was centrifuged at 2000 *g*, 20 °C for 5 min. Plasma was collected and stored at −80 °C until further analysis. Tumor-bearing scaffolds and organs (liver, spleen, kidneys, heart, lungs, femurs, sternum and brain) were excised, and imaged for fluorescence (Biospace Lab Photon Imager, Meyer instrument, USA), snap-frozen in liquid nitrogen and stored at −80 °C until further use. Fluorescence of Cy7-PM was detected in plasma and tissue homogenates by a fluorescence scanner Odyssey® (LI-COR Westburg, the Netherlands). Plasma was diluted with PBS prior to fluorescence detection. Frozen tissues were transferred to tubes with ceramic beads, weighed and homogenized in RIPA lysis buffer (20–188, Merck Millipore) (100 μL of buffer per 100 mg of tissue) using a Precellys 24 bead mill homogenizer (Bertin Instruments, France) for 60 s at 6000 rotation per minute (rpm). Homogenates were then centrifuged at 12,000 xg for 10 min and supernatants were analyzed for fluorescence. A calibration curve was prepared with Cy7-labeled polymer dissolved in DMSO and subsequently diluted in PBS or RIPA buffer at concentrations between 0.01 and 100 μg/mL.

2.4.2. Therapeutic efficacy of carfilzomib formulations

RAG2$^{-/-}\gamma c^{-/-}$ mice bearing human bone-like scaffolds, described in section 2.4, were treated with CFZ formulations. Bioluminescence imaging (BLI) (Biospace Lab Photon Imager, Meyer instrument, USA) was performed before start of the treatment (day 0). Based on BLI signals, mice were randomized into the following groups: phosphate buffered saline (PBS) ($n = 4$), CFZ-CD 4 mg/kg (n = 4) and CFZ-PM 4 mg/kg (n = 4). All treatments were administered i.v. *via* tail vein twice a week for a total of five injections. BLI was performed once weekly up to four weeks from start of the treatment. Body weight was monitored throughout the study. Animals were sacrificed when humane endpoint was reached, *i.e.* 20% decrease in body weight compared to the start of treatment, or when cumulative tumor volume > 10% of body weight (measured by digital caliper, Mitutoyo, Japan).

2.5. Statistical analysis

Data of *in vitro* cytotoxicity experiments were analyzed with GraphPad Prism 7.04 non-linear regression (GraphPad Software, Inc., La Jolla, CA, USA).

3. Results and discussion

3.1. Micelles characteristics: loading and release

CFZ was loaded at feed concentration of 1 mg/mL in 30 mg/mL PM using a nanoprecipitation method. CFZ-PM had an average diameter of 55 nm and polydispersity index (PDI) below 0.1, (Table 1). Bagheri et al. also reported average diameter of 55 nm for empty PM based on mPEG-b-p(HPMA-Bz) at the same polymer concentration (Bagheri et al., 2018). A similar size range was reported by Park et al. for micelles based on poly(ethylene glycol)-poly(caprolactone) (PEG-PCL) copolymers (Park et al., 2017). The small diameter of CFZ-PM is beneficial for long circulation in the blood stream (Wang et al., 2013a, 2013b), as well as for tumor penetration (Cabral et al., 2011; Sun et al., 2017). Further, the PEG shell creates a protective layer able to delay opsonization by plasma proteins and as a result can evade recognition by the mononuclear phagocytic system. Importantly, the size of CFZ-PM described here is reported to be advantageous for BM targeting (Deshantri et al., 2018). The reticuloendothelial sinusoidal blood capillaries contain pores with diameters of 60 nm, indicating that nanomedicines below this size can permeate into the BM interstitium.

Table 1
- Characteristics of polymeric micelles loaded with carfilzomib.

	Size (d.nm)[a]	PDI[a]	Encapsulation efficiency (%)[b]	Loading Content (%)[b]
carfilzomib micelles	54.7 ± 1.4	0.08 ± 0.02	88.4 ± 16.7	2.9 ± 0.5

Characteristics presented for CFZ-PM prepared at feed concentration of 1 mg/mL of carfilzomib.
Data are presented as mean ± SD, $n \geq 3$.
[a] Determined by DLS.
[b] Determined by UPLC.

CFZ was efficiently loaded in PM at feed concentration of 1 mg/mL of CFZ, the encapsulation efficiency was close to 90% and the loading content was around 3% in weight (Table 1). Ao et al. prepared CFZ micelles with a PEG-PCL block copolymer of different molecular weight of PCL block (2.3 or 5.5 kDa) and a fixed molecular weight of PEG (5 kDa). The best loading content (4% in weight) was achieved with the small PCL block (2.3 kDa) at 1: 10 feed weight ratio of drug and polymer, respectively (Ao et al., 2015). In this work, best loading content found for CFZ-PM was of 4% (data not shown) in weight at a feed ratio 1.5:30 between drug and polymer. CFZ loaded in PM presents improved water solubility (2.4 mg/mL) over free CFZ (near insoluble) and shows similar solubility in Captisol® (2 mg/mL).

Loading of CFZ in PM improves its solubility over free CFZ as it is near insoluble (FDA 2012).

The *in vitro* retention of CFZ in the core of PM was assessed with a method previously reported (Naksuriya et al., 2015). A dispersion of CFZ-PM was placed inside a dialysis cassette and dialyzed against PBS containing 2% (*v*/v) Triton™ X-100. This surfactant forms micelles in water which solubilize hydrophobic molecules and thus acting as a sink for the released drug (Naksuriya et al., 2015). Furthermore, Triton™ X-100 micelles did not mix with polymeric micelles (Naksuriya et al., 2015). At 24 h after incubation with Triton™ X-100 at 4 and 37 °C, 67 and 40% of CFZ retained in the micelles, respectively (Table 2). The highest release was observed at 37 °C which can be attributed to higher solubility of CFZ molecules in water at higher temperatures which aids to the transfer of CFZ molecules from the hydrophobic core of the micelles to the aqueous environment containing the Triton™ X-100 micelles. Curiously, retention in PBS at 37 °C (without the presence of any acceptor for hydrophobic compounds in the aqueous medium) revealed that only 50% of the micellar content was retained in the micelles.

Table 2
In vitro retention of carfilzomib in polymeric micelles after incubation in different media for 24 h.

	PBS 37 °C	2% (v/v) TritonX 4 °C	2% (v/v) TritonX 37 °C	4% (*w*/*v*) albumin 37 °C
Carfilzomib micelles	50 ± 13	67 ± 11	40 ± 17	22 ± 1

Data are presented as mean ± SD, $n = 3$ for Triton™ X-100, $n = 2$ for albumin and PBS.

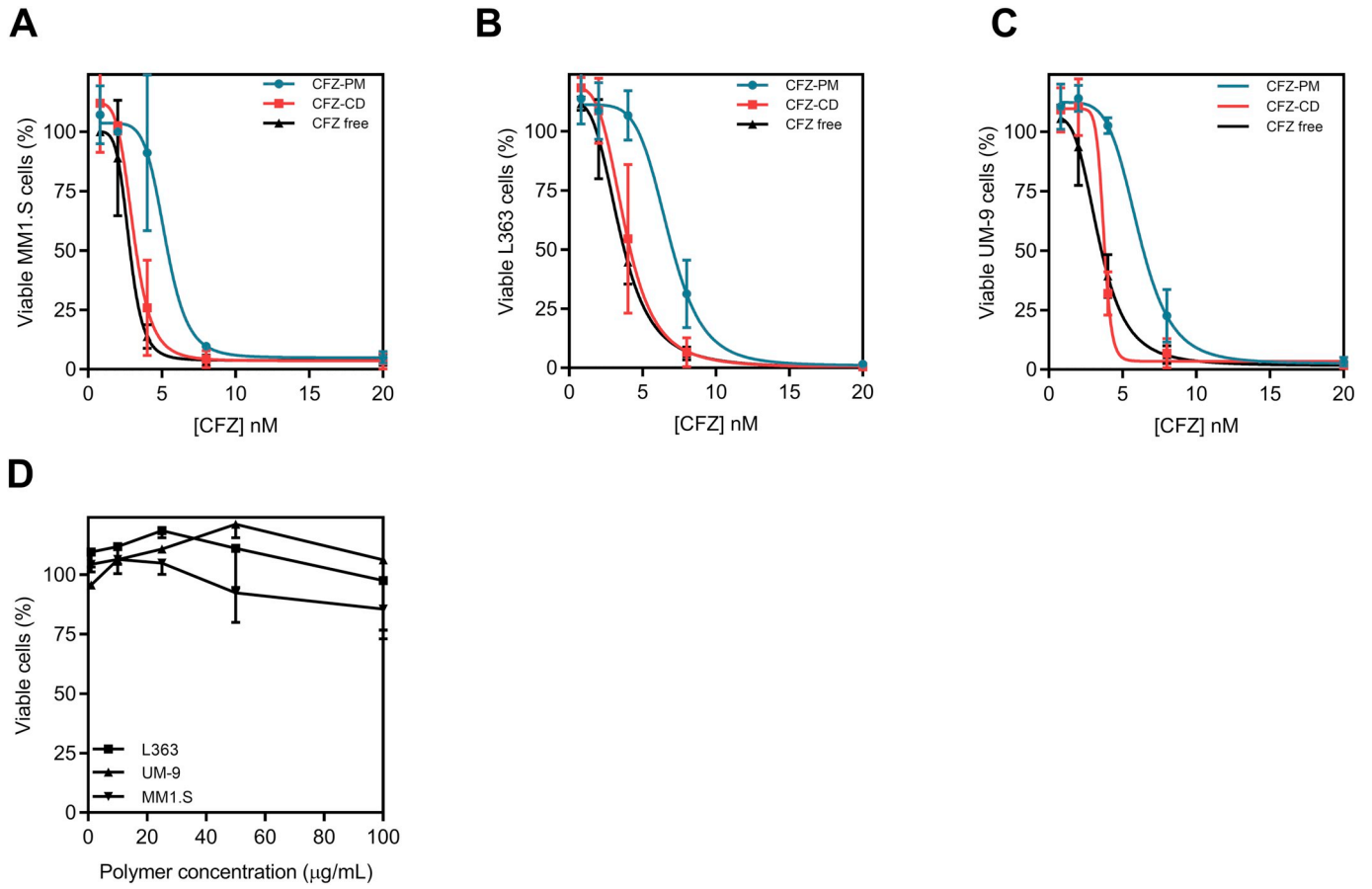

Fig. 3. Viability of MM cell lines after incubation with free carfilzomib, carfilzomib formulations and empty formulations for 48 h at 37°C and 5% CO_2. (A) MM.1S, (B) L363 and (C) UM-9 cells were treated in triplicates with increasing concentrations of carfilzomib solubilized in DMSO (CFZ free), in sulfobutylether β-cyclodextrin (CFZ-CD) or in polymeric micelles (CFZ-PM); (D) MM.1S, L363 and UM-9 cells incubated with empty polymeric micelles, at polymer concentrations between 0 and 100 μg/mL. After incubation, beetle luciferin was added to the wells at a final concentration of 3 mM. Ten minutes later, luminescence was detected. Percentage of viable cells was calculated compared to control (untreated) wells. Data is expressed as mean ± SD, n ≥ 3.

Release (based on dialysis) was also performed in the presence of albumin since this is the most abundant protein in plasma and has hydrophobic pockets to accommodate hydrophobic drugs (Kim et al., 2010; Rehman and Khan, 2015). In contrast with Triton™ X-100, CFZ was faster released when incubated with albumin, with only 40% of CFZ in PM (data not shown) after 2 h of incubation. Upon 24 h incubation with albumin at 37 °C, 22% of the initial CFZ loading was retained by micelles (Table 2) which is half of the percentage found after incubation with Triton™ X-100 at the same temperature. These figures suggest that albumin is expected to better predict the release profile after i.v. injection of these formulations.

3.2. In vitro cytotoxicity of carfilzomib-loaded polymeric micelles

The effect of CFZ-PM on the cellular viability of MM cell lines (MM1.S, L363 and UM-9) was evaluated. CFZ-CD and CFZ free (solubilized in DMSO) were also tested. CFZ-PM, CFZ-CD and CFZ free showed a dose dependent cytotoxic effect towards MM cell lines at the nanomolar range, which indicates the potency of CFZ (Fig. 3 A, B and C). The IC_{50} of CFZ-PM was of 5.3, 6.8 and 6.1 nM in MM1.S, L363 and UM-9 cells, respectively. For CFZ-CD and free CFZ, IC_{50} values were slightly lower (Table 3). The higher IC_{50} of CFZ-PM, compared to CFZ-CD and free CFZ, can be attributed to CFZ retention in the core of the PM and thus leads to a delayed/minor cytotoxic effect of the formulation. As a control, the effect of empty PM on the viability of MM cells was also determined (Fig. 3D). For the concentrations tested, close to 100% of cells remained viable which is in line with the observed cytocompatibility of empty micelles upon incubation with adherent cell lines (Shi et al., 2015).

Table 3
IC_{50} (in nM) of carfilzomib formulations upon 48 h incubation with MM cells.

	MM1.S	L363	UM-9
CFZ-PM	5.3	6.8	6.1
CFZ-CD	3.1	3.8	3.7
CFZ free	2.8	3.5	3.4

3.3. In vivo circulation and biodistribution of Cy7-labeled PM

To investigate the potential of PM as a delivery system with extended circulation time after systemic administration and targeted tissue distribution, huBMsc mice xenografted with MM.1S cells were i.v. injected with empty Cy7-PM. Blood concentrations of Cy7-PM were assessed at 1, 2, 4 and 24 h after injection whereas the tissue distribution of the labeled micelles was quantified 4 and 24 h post-injection. Cy7-PM showed a long circulation time with 80% of the injected dose (ID) in circulation 24 h after injection (Fig. 4 A). With the same micellar system, Shi et al. reported around 20% ID in a solid tumor mouse model (CD-1 mice) (Shi et al., 2015) and Alaarg et al. reported 10%ID/g of tissue on a mouse model of advanced atherosclerosis ($Apoe^{-/-}$ mice) (Alaarg et al., 2017), at the same time point post-injection. These differences in circulation times can be attributed to the different mouse strains used in the different models applied in the

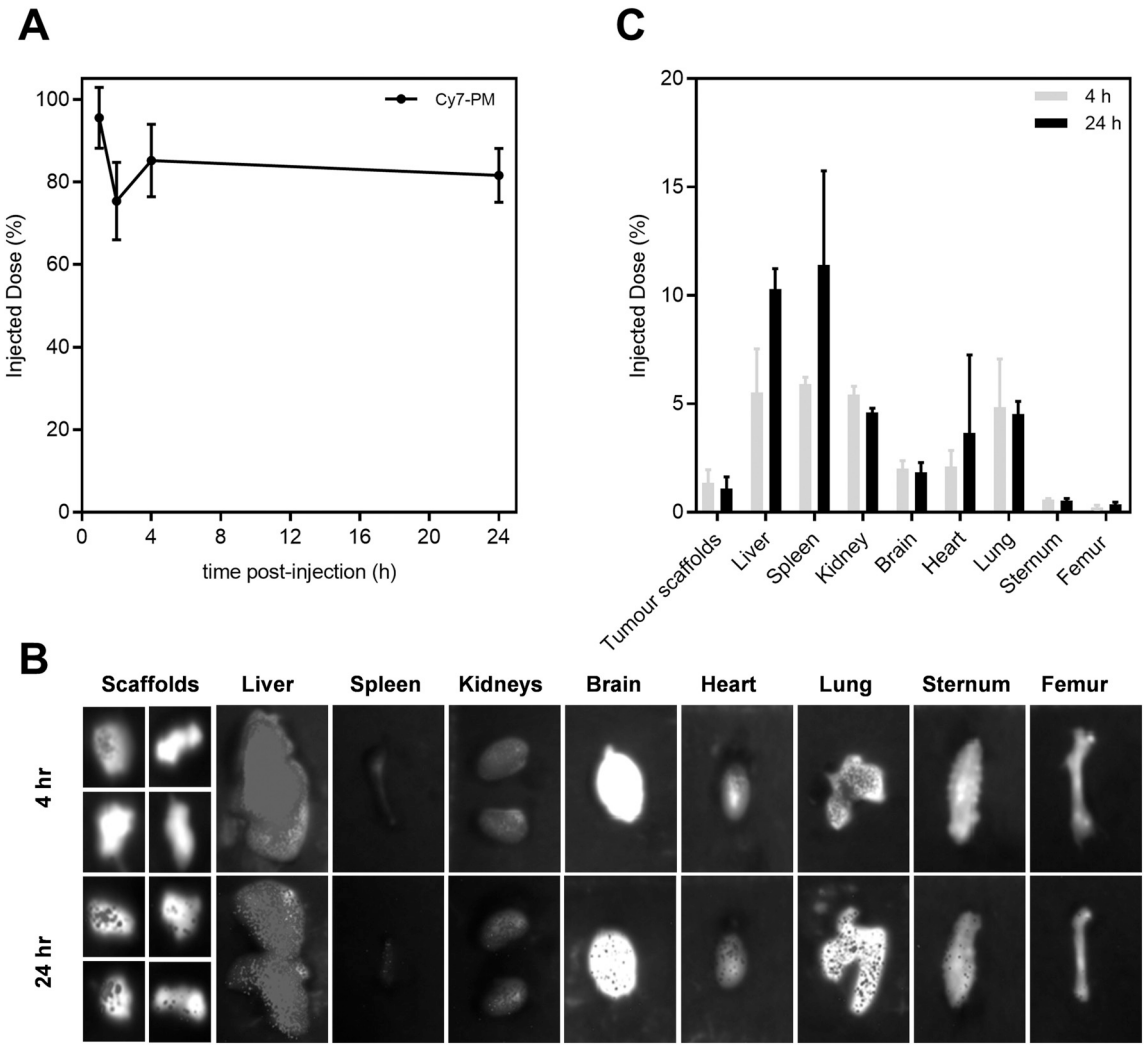

Fig. 4. Blood circulation kinetics and distribution in tumor-bearing scaffolds & tissues of Cy7-labeled polymeric micelles on a "humanized" bone marrow-like scaffold model. (A) Circulation of Cy7-PM in blood at different timepoints after injection (1, 2, 4 and 24 h), expressed as % of Injected dose (ID) present in circulation. Blood collected immediately after injection was considered as 100% ID. Fluorescence intensity in plasma samples was measured in Odyssey® imager; (B) Images of scaffolds and tissues 4 and 24 h after i.v. injection of Cy7-PM. Tissues were excised and imaged using BiospaceLab Photon Imager; (C) Scaffolds and tissue distribution of Cy7-PM at 4 and 24 h after i.v. injection. Cy7-PM accumulation was determined after homogenization of the scaffolds and tissues. Fluorescence present in the homogenates was measured with Odyssey® imager. Data is expressed as mean ± SD, n = 3 per time point, n(scaffolds) > 5 per time point.

different studies. Moreover, PM prepared here present average hydrodynamic diameter of 50 nm whereas in the above mentioned studies, mPEG-b-p(HPMA-Bz) based micelles had sizes of 100 (Shi et al., 2015) or 80 nm (Alaarg et al., 2017). Additionally, the RAG2$^{-/-}\gamma c^{-/-}$ mice used in the present work have an almost absent immune system (Mazurier et al., 1999) – *i.e.* no T, B or NK cells and only tissue macrophages were present in this model. The absence of these immune cells likely limits recognition and subsequent clearance of the polymeric micelles by the mononuclear phagocyte system. Similarly, we recently reported prolonged circulation times of liposomes in RAG2$^{-/-}\gamma c^{-/-}$ mice compared to other mouse models (involving different mouse strains) (Deshantri et al., 2019) indicating that this phenomenon also applies to other nanoparticle types.

Scaffolds and organs were imaged for fluorescence analysis (Fig. 4 B). Tumor-bearing scaffolds showed accumulation of Cy7-PM at both time points evaluated (4 and 24 h) with around 1% of the ID in the tumors (Fig. 4C). In kidneys and lungs, Cy7-PM were also detected, however, in these organs the signal might indicate that the localization can be ascribed to circulating PM still present in blood. Highest accumulation of Cy7-PM was found in liver and spleen (10 and 11% ID, respectively) which are macrophage-rich organs, responsible for the clearance of nanosized particles (Ernsting et al., 2013). Besides this, liver is a highly vascularized organ and thus part of the PM's disposition can be attributed to micelles still in blood circulation inside the liver. Although the spleen is not the primary target organ in MM, spleen involvement is observed in 30% of MM patients (Saboo et al., 2012). Therefore, one can take advantage of high accumulation of Cy7-PM in the spleen. The presence of fluorescence from Cy7-PM in the kidney can be due to accumulation of polymer chain unimers with which micelles are in equilibrium (Etrych et al., 2012; Shi et al., 2015). An alternative explanation is that renal damage occurred in this model, a typical complication also in clinical MM, due to the accumulation of light chains of antibodies leading to local inflammation (Davenport and Merlini, 2012).

3.4. Tolerability and therapeutic potential of carfilzomib-loaded polymeric micelles

The tolerability and therapeutic potential of CFZ-PM were evaluated in the huBMsc model xenografted with MM1.S cells. Twelve days after myeloma tumor cells inoculation into the huBMsc, treatment was started. Each mouse received two injections per week for a total of five

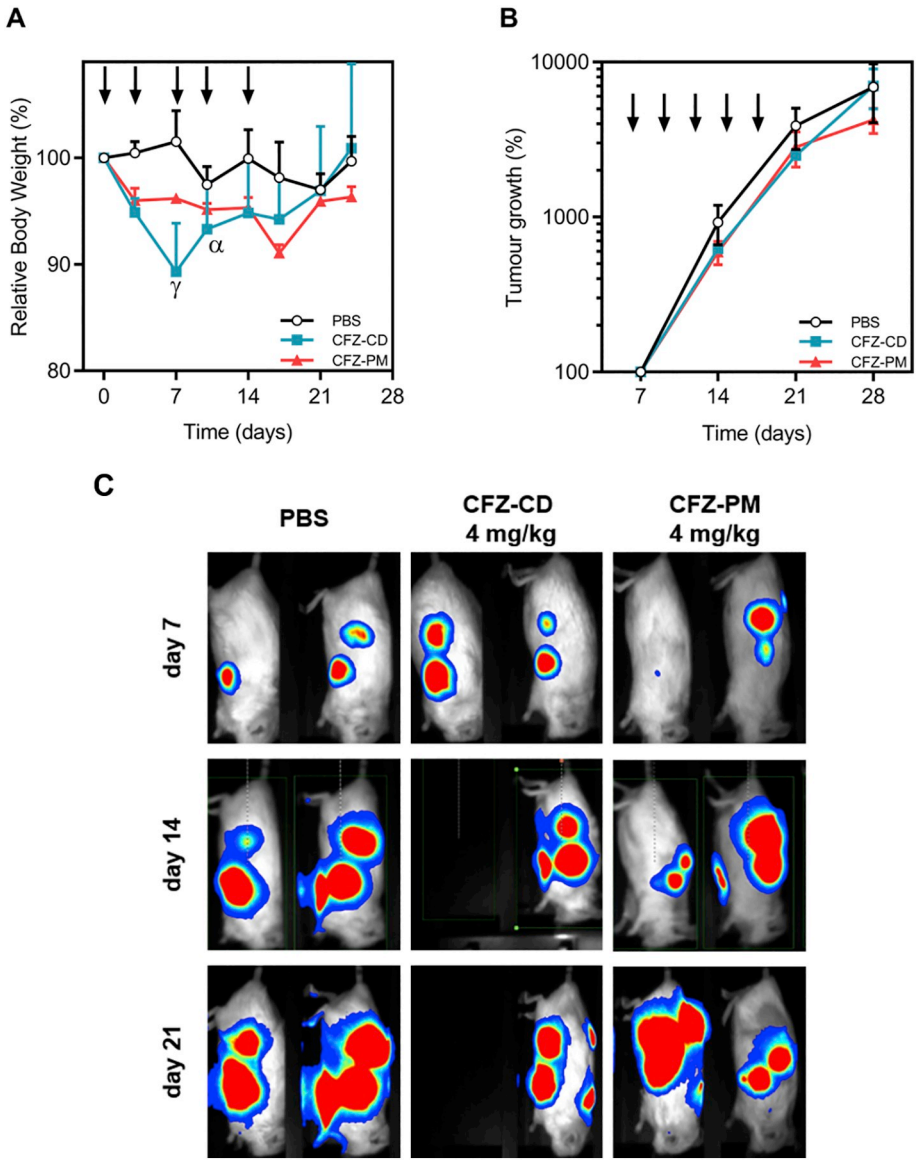

Fig. 5. Effect of carfilzomib loaded polymeric micelles versus carfilzomib in sulfobutylether β-cyclodextrin on tumor growth of a "humanized" bone marrow-like scaffold model. Mice bearing four human bone containing scaffolds were inoculated with luciferase labeled MM1.S cells into the scaffolds. Twelve days after inoculation of tumor cells, animals were treated with PBS, CFZ-CD or CFZ-PM, both at 4 mg/kg. Arrows represent i.v. injections. Bioluminescence imaging (BLI) was performed weekly. (A) Relative body weight of the mice throughout the experiment. γ - body weight of 3 out of 4 mice and α – body weight of 2 out of 4 mice; (B) Percentage of tumor growth compared to the day when treatment started. Tumor growth % was determined through analysis of BLI of each scaffold as counts per minute (cpm), and 100% tumor growth considered on day 0 – start of the treatment; (C) BLI images of representative mice 7 days (top panels), 14 days (middle panels) and 21 days (bottom panels) after treatment initiation. Fifty percent of animals treated with CFZ-CD needed to be culled from the experiment due to toxicity. Data are presented as mean ± SEM, n = 4 per group.

injections. In this study, CFZ-PM was compared with the clinically approved formulation of carfilzomib - which is CFZ loaded in sulfobutylether β-cyclodextrin, *i.e.* Kyprolis® - at a dose close (and below) to previously reported MTD for CFZ in mice (Nooka et al., 2013). To evaluate peripheral toxicity due to the administered treatments, we monitored the body weight of the treated mice throughout the study (Fig. 5 A). The PM-treated group showed a moderate reduction in body weight (< 5%) during the first week after which no further weight reduction was observed during the remainder of the experiment. On the other hand, Kyprolis® was not well tolerated and resulted in half of the mice in this group with more than 20% weight loss after one week of treatment (2 injections). These mice needed to be humanely killed since the humane end point was reached. This indicates that the maximum tolerated dose for Kyprolis® was met in this huBMsc mouse model whereas CFZ-PM formulation might have been administered in a higher dose than the one applied. Tumor growth was followed by weekly bioluminescence imaging (BLI) and showed growth in all treatment groups (Fig. 5 B and C). For BLI of all scaffolds and percentage of tumor growth of individual scaffolds we refer to Fig. S1 and S2, respectively. As in the present study, Park et al. did not find superior antitumor activity of CFZ loaded in PEG-PCL polymeric micelles over CFZ-CD in a human lung cancer xenograft mouse model (Park et al., 2017). Furthermore, they also reported systemic toxicity in mice treated with 6 mg/kg of CFZ-CD, where 4 out of 6 mice died, whereas no toxicity was found for mice treated with CFZ-PM at the same dose.

The improvement of the tolerability is an important step in the treatment of MM as it may allow the use of higher doses that can be expected to be more efficacious. The micellar stability and drug retention in PM after intravenous administration are also critical aspects in the development of successful drug delivery systems. Long circulation and adequate drug retention in PM are key to ensure that sufficient drug levels reach tumor/target site. PM showed good colloidal stability with long circulation times in blood (80% ID 24 h after injection). In this study, the pharmacokinetic profile of CFZ when loaded in PM was not evaluated. Still, the *in vitro* release of CFZ from PM when in contact with albumin suggests a fast clearance of CFZ. The presumed fast clearance of CFZ *in vivo is* expected to cause the lack of therapeutic efficacy observed. Importantly, whereas the *in vitro* experiments indicate sensitivity of the MM cell line, this sensitivity is apparently lost *in vivo*. This underlines the importance of drug screening in advanced models that resemble the complexity of human tumors to fully appreciate the complexity of treatment.

4. Conclusions

In the present work, CFZ was efficiently loaded in the core of polymeric micelles. The micelles have a favorable size (55 nm) for long circulation upon systemic injection and for passive targeting of tissues with increased capillary permeability. This was confirmed by evaluation of the circulation times of labeled micelles, with more than 80% of ID still present in the circulation after 24 h, which might partly be explained by the immune status of the RAG2$^{-/-}\gamma c^{-/-}$ mouse strain used in this study. Increase in PM accumulation over time was observed in tumor-bearing scaffolds as well as in macrophage-rich organs such as the liver and spleen. The effects on tumor growth delay in a "humanized" BM-like scaffold model were absent, but similar to what was found for the clinically approved formulation - Kyprolis® - dosed at the MTD. In addition, and importantly, the tolerability of the formulation presented in this work was substantially better than that of Kyprolis®, which indicates that higher doses and/or more frequent treatment could be pursued.

Funding

This work was funded by Netherlands Organization for Scientific Research (NWO), High Tech Systems & Materials grant number 13312.

Role

Aida Varela-Moreira, Demian van Straten, Heleen F. van Leur, Ruud W.J. Ruiter, Anil K. Deshantri were responsible for experimental work, data processing and data analysis,

Aida Varela-Moreira, Wim E. Hennink, Marcel H.A.M. Fens, Richard W.J. Groen, and Raymond M. Schiffelers were responsible for the conception and design of the work and interpretation of the data and drafting the manuscript.

Declaration of Competing Interest

The authors report no conflicts of interest.

References

Adams, J., 2004. The proteasome: A suitable antineoplastic target. Nat. Rev. Cancer 4, 349–360.
FDA, U. S. F. A. D. A, 2012. Kyprolis™ (carfilzomib) for injection.
Alaarg, A., Senders, M.L., Varela-Moreira, A., Perez-Medina, C., Zhao, Y., Tang, J., Fay, F., Reiner, T., Fayad, Z.A., Hennink, W.E., Metselaar, J.M., Mulder, W.J.M., Storm, G., 2017. A systematic comparison of clinically viable nanomedicines targeting hmg-coa reductase in inflammatory atherosclerosis. J. Control. Release 262, 47–57.
Andreu-Vieyra, C., Berenson, J.R., 2014. Carfilzomib in multiple myeloma. Expert. Opin. Biol. Ther. 14, 1685–1699.
Ao, L., Reichel, D., Hu, D., Jeong, H., Kim, K.B., Bae, Y., Lee, W., 2015. Polymer micelle formulations of proteasome inhibitor carfilzomib for improved metabolic stability and anticancer efficacy in human multiple myeloma and lung cancer cell lines. J. Pharmacol. Exp. Ther. 355, 168.
Azaïs, I., Brault, R., Debiais, F., 2010. New treatments for myeloma. Joint Bone Spine. 77, 20–26.
Bagheri, M., Bresseleers, J., Varela-Moreira, A., Sandre, O., Meeuwissen, S.A., Schiffelers, R.M., Metselaar, J.M., van Nostrum, C.F., van Hest, J.C.M., Hennink, W.E., 2018. Effect of formulation and processing parameters on the size of mpeg-b-p(hpma-bz) polymeric micelles. Langmuir. 34, 15495–15506.
Cabral, H., Matsumoto, Y., Mizuno, K., Chen, Q., Murakami, M., Kimura, M., Terada, Y., Kano, M.R., Miyazono, K., Uesaka, M., Nishiyama, N., Kataoka, K., 2011. Accumulation of sub-100 nm polymeric micelles in poorly permeable tumours depends on size. Nat. Nanotechnol. 6, 815–823.
Davenport, A., Merlini, G., 2012. Myeloma kidney: advances in molecular mechanisms of acute kidney injury open novel therapeutic opportunities. Nephrol. Dial. Transplant. 27, 3713–3718.
Deshantri, A.K., Varela Moreira, A., Ecker, V., Mandhane, S.N., Schiffelers, R.M., Buchner, M., Fens, M., 2018. Nanomedicines for the treatment of hematological malignancies. J. Control. Release 287, 194–215.
Deshantri, A.K., Fens, M.H., Ruiter, R.W.J., Metselaar, J.M., Storm, G., van Bloois, L., Varela-Moreira, A., Mandhane, S.N., Mutis, T., Martens, A.C.M., Groen, R.W.J., Schiffelers, R.M., 2019. Liposomal dexamethasone inhibits tumor growth in an advanced human-mouse hybrid model of multiple myeloma. J. Control. Release 296, 232–240.
Ernsting, M.J., Murakami, M., Roy, A., Li, S.D., 2013. Factors controlling the pharmacokinetics, biodistribution and intratumoral penetration of nanoparticles. J. Control. Release 172, 782–794.
Etrych, T., Subr, V., Strohalm, J., Sirova, M., Rihova, B., Ulbrich, K., 2012. Hpma copolymer-doxorubicin conjugates: the effects of molecular weight and architecture on biodistribution and in vivo activity. J. Control. Release 164, 346–354.
Gandolfi, S., Laubach, J.P., Hideshima, T., Chauhan, D., Anderson, K.C., Richardson, P.G., 2017. The proteasome and proteasome inhibitors in multiple myeloma. Cancer Metastasis Rev. 36, 561–584.
Groen, R.W.J., Noort, W.A., Raymakers, R.A., Prins, H.-J., Aalders, L., Hofhuis, F.M., Moerer, P., van Velzen, J.F., Bloem, A.C., van Kessel, B., Rozemuller, H., van Binsbergen, E., Buijs, A., Yuan, H., de Bruijn, J.D., de Weers, M., Parren, P.W.H.I., Schuringa, J.J., Lokhorst, H.M., Mutis, T., Martens, A.C.M., 2012. Reconstructing the human hematopoietic niche in immunodeficient mice: Opportunities for studying primary multiple myeloma. Blood. 120, e9–e16.
Gu, Z., Wang, X., Cheng, R., Cheng, L., Zhong, Z., 2018. Hyaluronic acid shell and disulfide-crosslinked core micelles for in vivo targeted delivery of bortezomib for the treatment of multiple myeloma. Acta Biomater. 80, 288–295.
Harvey, R., 2014. Incidence and management of adverse events in patients with relapsed and/or refractory multiple myeloma receiving single-agent carfilzomib. Clin. Pharm. 6, 87–96.
Herndon, T.M., Deisseroth, A., Kaminskas, E., Kane, R.C., Koti, K.M., Rothmann, M.D., Habtemariam, B., Bullock, J., Bray, J.D., Hawes, J., Palmby, T.R., Jee, J., Adams, W., Mahayni, H., Brown, J., Dorantes, A., Sridhara, R., Farrell, A.T., Pazdur, R., 2013. U.S. Food and drug administration approval: Carfilzomib for the treatment of multiple myeloma. Clin. Cancer Res. 19, 4559.
Kim, S., Shi, Y., Kim, J.Y., Park, K., Cheng, J.X., 2010. Overcoming the barriers in micellar drug delivery: Loading efficiency, in vivo stability, and micelle-cell interaction. Expert Opin Drug Deliv. 7, 49–62.
Kumar, S.K., Lee, J.H., Lahuerta, J.J., Morgan, G., Richardson, P.G., Crowley, J., Haessler, J., Feather, J., Hoering, A., Moreau, P., LeLeu, X., Hulin, C., Klein, S.K., Sonneveld, P., Siegel, D., Blade, J., Goldschmidt, H., Jagannath, S., Miguel, J.S., Orlowski, R., Palumbo, A., Sezer, O., Rajkumar, S.V., Durie, B.G., 2012. Risk of progression and survival in multiple myeloma relapsing after therapy with imids and bortezomib: a multicenter international myeloma working group study. Leukemia. 26, 149–157.
Manier, S., Sacco, A., Leleu, X., Ghobrial, I.M., Roccaro, A.M., 2012. Bone marrow microenvironment in multiple myeloma progression. J. Biomed. Biotechnol. 2012, 157496.
Mazurier, F., Fontanellas, A., Salesse, S., Taine, L., Landriau, S., Moreau-Gaudry, F., Reiffers, J., Peault, B., Di Santo, J.P., de Verneuil, H., 1999. A novel immunodeficient mouse model–rag2 x common cytokine receptor gamma chain double mutants–requiring exogenous cytokine administration for human hematopoietic stem cell engraftment. J. Interf. Cytokine Res. 19, 533–541.
Naksuriya, O., Shi, Y., van Nostrum, C.F., Anuchapreeda, S., Hennink, W.E., Okonogi, S., 2015. Hpma-based polymeric micelles for curcumin solubilization and inhibition of cancer cell growth. Eur. J. Pharm. Biopharm. 94, 501–512.
Nooka, A., Gleason, C., Casbourne, D., Lonial, S., 2013. Relapsed and refractory lymphoid neoplasms and multiple myeloma with a focus on carfilzomib. Biologics. 7, 13–32.
Okazuka, K., Ishida, T., 2018. Proteasome inhibitors for multiple myeloma. Jpn. J. Clin. Oncol. 48, 785–793.
Palumbo, A., Anderson, K., 2011. Multiple myeloma. N. Engl. J. Med. 364, 1046–1060.
Papadopoulos, K.P., Burris, H.A., Gordon, M., Lee, P., Sausville, E.A., Rosen, P.J., Patnaik, A., Cutler, R.E., Wang, Z., Lee, S., Jones, S.F., Infante, J.R., 2013. A phase i/ii study of carfilzomib 2–10-min infusion in patients with advanced solid tumors. Cancer Chemother. Pharmacol. 72, 861–868.
Papadopoulos, K.P., Siegel, D.S., Vesole, D.H., Lee, P., Rosen, S.T., Zojwalla, N., Holahan, J.R., Lee, S., Wang, Z., Badros, A., 2015. Phase i study of 30-minute infusion of carfilzomib as single agent or in combination with low-dose dexamethasone in patients with relapsed and/or refractory multiple myeloma. J. Clin. Oncol. 33, 732–739.
Park, J.E., Chun, S.E., Reichel, D., Min, J.S., Lee, S.C., Han, S., Ryoo, G., Oh, Y., Park, S.H., Ryu, H.M., Kim, K.B., Lee, H.Y., Bae, S.K., Bae, Y., Lee, W., 2017. Polymer micelle formulation for the proteasome inhibitor drug carfilzomib: Anticancer efficacy and pharmacokinetic studies in mice. PLoS One 12, e0173247.
Prins, H.-J., Rozemuller, H., Vonk-Griffioen, S., Verweij, V.G.M., Dhert, W.J.A., Slaper-Cortenbach, I.C.M., Martens, A.C.M., 2009. Bone-forming capacity of mesenchymal stromal cells when cultured in the presence of human platelet lysate as substitute for fetal bovine serum. Tissue Eng. A 15, 3741–3751.
Rehman, M.T., Khan, A.U., 2015. Understanding the interaction between human serum albumin and anti-bacterial/ anti-cancer compounds. Curr. Pharm. Des. 21, 1785–1799.
Roodman, G.D., 2009. Pathogenesis of myeloma bone disease. Leukemia 23, 435–441.
Saboo, S.S., Krajewski, K.M., O'Regan, K.N., Giardino, A., Brown, J.R., Ramaiya, N., Jagannathan, J.P., 2012. Spleen in haematological malignancies: Spectrum of imaging findings. Br. J. Radiol. 85, 81–92.
Sestak, V., Roh, J., Klepalova, L., Kovarikova, P., 2016. A uhplc-uv-qtof study on the stability of carfilzomib, a novel proteasome inhibitor. J. Pharm. Biomed. Anal. 124, 365–373.
Shi, Y., van der Meel, R., Theek, B., Oude Blenke, E., Pieters, E.H., Fens, M.H., Ehling, J., Schiffelers, R.M., Storm, G., van Nostrum, C.F., Lammers, T., Hennink, W.E., 2015.

Complete regression of xenograft tumors upon targeted delivery of paclitaxel via pi-pi stacking stabilized polymeric micelles. ACS Nano 9, 3740–3752.
Sun, Q., Ojha, T., Kiessling, F., Lammers, T., Shi, Y., 2017. Enhancing tumor penetration of nanomedicines. Biomacromolecules. 18, 1449–1459.
Wang, B., He, X., Zhang, Z., Zhao, Y., Feng, W., 2013a. Metabolism of nanomaterials in vivo: Blood circulation and organ clearance. Acc. Chem. Res. 46, 761–769.
Wang, Z., Yang, J., Kirk, C., Fang, Y., Alsina, M., Badros, A., Papadopoulos, K., Wong, A., Woo, T., Bomba, D., Li, J., Infante, J.R., 2013b. Clinical pharmacokinetics, metabolism, and drug-drug interaction of carfilzomib. Drug Metab. Dispos. 41, 230–237.
Yang, J., Wang, Z., Fang, Y., Jiang, J., Zhao, F., Wong, H., Bennett, M.K., Molineaux, C.J., Kirk, C.J., 2011. Pharmacokinetics, pharmacodynamics, metabolism, distribution, and excretion of carfilzomib in rats. Drug Metab. Dispos. 39, 1873–1882.
Yuan, H., Van Den Doel, M., Li, S., Van Blitterswijk, C.A., De Groot, K., De Bruijn, J.D., 2002. A comparison of the osteoinductive potential of two calcium phosphate ceramics implanted intramuscularly in goats. J. Mater. Sci. Mater. Med. 13, 1271–1275.